

Spurious microwave crosstalk in floating superconducting circuits

Peng Zhao,^{1,*} Yingshan Zhang,¹ Xuegang Li,¹ Jiaxiu Han,¹ Huikai Xu,¹ Guangming Xue,^{1,†} Yirong Jin,¹ and Haifeng Yu¹

¹Beijing Academy of Quantum Information Sciences, Beijing 100193, China

(Dated: June 23, 2022)

Crosstalk is a major concern in the implementation of large-scale quantum computation since it can degrade the performance of qubit addressing and cause gate errors. Finding the origin of crosstalk and separating contributions from different channels are essential prerequisites for figuring out crosstalk mitigation schemes. Here, by performing circuit analysis of two coupled floating transmon qubits, we demonstrate that, even if the stray coupling, e.g., between a qubit and the drive line of its nearby qubit, is absent, microwave crosstalk between qubits can still exist due to the presence of a spurious crosstalk channel. This channel arises from free modes, which are supported by the floating structure of transmon qubits, i.e., the two superconducting islands of each qubit with no galvanic connection to the ground. For various geometric layouts of floating transmon qubits, we give the contributions of microwave crosstalk from the spurious channel and show that this channel can become a performance-limiting factor in qubit addressing. This research could provide guidance for suppressing microwave crosstalk between floating superconducting qubits through the design of qubit circuits.

I. INTRODUCTION

Integrating a growing number of qubits without sacrificing quantum gate performance is a key task in the implementation of large-scale quantum computers with superconducting qubits [1]. One of the main obstacles that needs to be overcome, in this task, is crosstalk, including classical crosstalk due to unintended classical electromagnetic couplings [2–8] and quantum crosstalk arising from residual quantum coupling [5, 9–12], which can make qubit addressing a challenge [9] and degrade gate performance in multiqubit quantum processors [13]. In this context, the progress in understanding and mitigating crosstalk has made indispensable contributions to the impressive achievements toward developing large-scale superconducting quantum computing over the past decade.

One of the most ubiquitous crosstalk for superconducting quantum processors is the microwave crosstalk, which describes that microwave drives applied to one qubit can cause unintended drives felt by the others. To address this issue, various active cancellation methods, i.e., one first characterizes it and then cancels it actively with a compensation drive, have been demonstrated [14, 15]. Nevertheless, mitigating the crosstalk at device level may complement existing active approaches and further reduce the needed physical resource, especially for large-scale quantum processors. Indeed, previous works show that the crosstalk can be suppressed at the device level, but only if the origin of the crosstalk and contributions from different crosstalk channels are well understood [2, 6].

Generally, to implement universal control over qubits in quantum processors, at least a single drive line (drive channel) per qubit is needed. Hence, as shown in Fig. 1, there are three possible microwave crosstalk channels in superconducting quantum processors, including (Type-1) stray coupling between the dedicated drive lines of qubits, the direct (Type-2) and the indirect (Type-3) coupling between one qubit and the drive line of others. For large-scale quantum processors, a

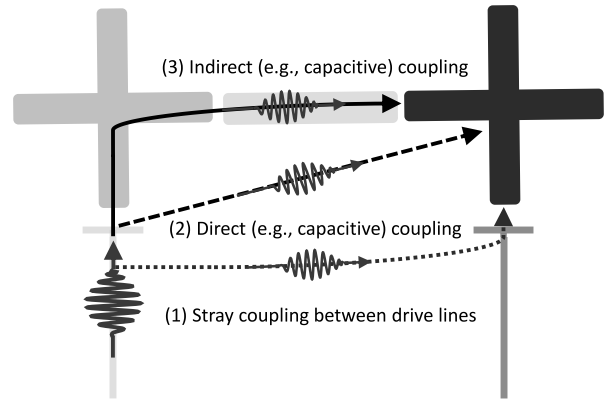


FIG. 1: Three possible channels of microwave crosstalk between two coupled superconducting qubits. Each qubit (cross-shaped) has a dedicated drive line (T-shaped) for single-qubit addressing. The two qubits are coupled via a coupler circuit (strip-shaped), such as a direct coupling capacitor or a bus coupler. Microwave crosstalk can arise from: (Type-1) the stray coupling between the two drive lines; (Type-2) the direct or (Type-3) indirect coupling between one qubit and the drive line of its neighbor.

high density of control wiring is required, thus the crosstalk through the first two channels could become more serious [2, 4, 6]. Generally, the two channels can be mitigated by improving the physical isolation between drive lines and qubits [4]. For the Type-3 channel, however, its physical origin and mitigation seems to be more nontrivial. In principle, its origin can be modeled by the indirect coupling between one qubit and the drive line of the others through an effective circuit network [16]. Physically, the circuit network could arise from the presence of package modes or chip modes [2, 4], and could even relate to the qubit itself [17, 18]. Nevertheless, the exact nature of this circuit network and its contribution to the microwave crosstalk are less studied.

In this work, we present a spurious microwave crosstalk

*Electronic address: shangniguo@sina.com

†Electronic address: xuegm@baqis.ac.cn

channel (Type-3) enabled by the presence of free modes in floating transmon circuits [19–22]. By performing circuit analysis of coupled floating transmon qubits with different geometric layouts [23–25], we show that the microwave crosstalk contributed from this spurious channel can become non-negligible, thus potentially limiting the performance of qubit addressing. More importantly, this crosstalk channel only depends on the qubit circuit itself, thus acting as an intrinsic channel, which can exist even when the stray coupling, e.g., between drive lines and qubits, is absent. This feature also suggests that this spurious channel can be mitigated through qubit circuit design.

This paper is organized as follows. In Sec. II, we analyze the quantum circuit of two direct-coupled floating transmon qubits (in the Appendix we further extended our analysis to the case, where floating transmon qubits are coupled via a grounded or floating bus coupler) and show that the presence of the free modes can induce a spurious microwave crosstalk channel. In Sec. III, for transmon qubits with different qubit geometric layouts, we give the contributions of microwave crosstalk from the spurious channel. In Sec. IV, we give discussions on the relation of the free-mode-mediated spurious crosstalk channel in our work with the free-mode mediated inter-qubit interactions illustrated in two recent works [26, 27] and show that the present work can be viewed as complements to the two earlier works, extending the free-mode mediated interactions from "quantum regime" (for inter-qubit coupling) to "semi-classical regime" (for classical microwave crosstalk). Finally, in Sec. V, we provide a summary of our work.

II. SPURIOUS MICROWAVE CROSSTALK CHANNEL

To understand the origin of the spurious microwave crosstalk channel, we consider a superconducting circuit comprising two direct-coupled floating transmon qubits (Q_1 and Q_2), and one of the two qubits (Q_1) is coupled capacitively to a voltage source, as shown in Fig. 2(a). When expressed in terms of the node flux variables Φ_j and $\phi_j = 2\pi\Phi_j/\Phi_0$ with Φ_0 the magnetic flux quantum, the circuit Lagrangian is given by (details on its derivation can be found in Appendix A) [28, 29]

$$\mathcal{L} = \frac{1}{2} \dot{\Phi}^T \mathbf{C} \dot{\Phi} + E_{J1} \cos(\phi_{1m}) + E_{J2} \cos(\phi_{2m}), \quad (1)$$

where $\Phi = (\Phi_d \Phi_{1p} \Phi_{1m} \Phi_{2p} \Phi_{2m})^T$ with $\Phi_{1p(m)} = \Phi_1 \pm \Phi_2$ and $\Phi_{2p(m)} = \Phi_3 \pm \Phi_4$, E_{J1} and E_{J2} are the Josephson energies, and \mathbf{C} denotes the capacitance matrix of the circuit. Accordingly, the circuit Hamiltonian can be constructed as $H = \sum_j Q_j \dot{\Phi}_j - E_{J1} \cos(\phi_{1m}) - E_{J2} \cos(\phi_{2m})$ with the charge variables $Q_j = \partial\mathcal{L}/\partial\dot{\Phi}_j$. Here, the modes associated with the variables Q_{1m} and Q_{2m} are the qubit modes, which have both the charge energy and the potential energy [22], while the modes associated with Q_{1p} and Q_{2p} , and which don't have potential terms in the Hamiltonian, are the free modes [19–21]. From the derivation and also mentioned in previous works [19–21], the presence of the free modes are supported by the floating structure of transmon qubits, i.e.,

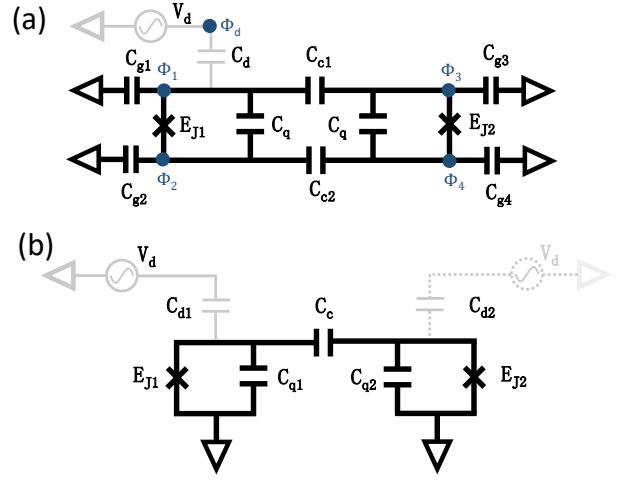


FIG. 2: (a) Schematic circuit diagram for two direct-coupled floating transmon qubits (Q_1 and Q_2), where a dedicated drive line (left) is coupled capacitively to one of the two qubits, i.e., Q_1 . After removing the free modes supported by the floating structure of qubits, the circuit can be transformed into an equivalent circuit shown in (b), where two grounded transmon qubits are coupled capacitively. Here, the virtual drive line (right, grey dashed line) is introduced to model the crosstalk due to the presence of a spurious channel.

the two superconducting islands of the qubit have no galvanic connection to the ground, as shown in Fig. 2(a), contributing to an additional quantum degree of freedom.

Since free modes actually don't participate in the circuit dynamics [19–21], one can drop the charge terms corresponding to the two free modes and rewrite the circuit Hamiltonian as

$$H_r = \frac{1}{2} \mathbf{Q}_r^T \mathbf{C}_r^{-1} \mathbf{Q}_r - E_{J1} \cos(\phi_{1m}) - E_{J2} \cos(\phi_{2m}), \quad (2)$$

with $\mathbf{Q}_r = (Q_d Q_{1m} Q_{2m})^T$. Here, \mathbf{C}_r denotes the reduced capacitance matrix, which can also be used to describe a circuit system consisting of two direct-coupled grounded transmon qubits, as shown in Fig. 2(b) (see Appendix A for details). Here, for illustration purpose, considering a typical case where all the island capacitors take a same capacitance, i.e., $C_{g1} = C_{g2} = C_{g3} = C_{g4} = C_g$ and both the island capacitance C_g and the shunt capacitance C_q largely exceed the coupling capacitances, i.e., $\{C_g, C_q\} \gg \{C_d, C_{c1}, C_{c2}\}$, the matrix \mathbf{C}_r can be approximated by

$$\mathbf{C}_r \approx \begin{pmatrix} C_d & -\frac{C_d}{2} & -\frac{C_d(C_{c1}-C_{c2})}{4C_g} \\ -\frac{C_d}{2} & C_q + \frac{C_g}{2} & -\frac{C_{c1}+C_{c2}}{4} \\ -\frac{C_d(C_{c1}-C_{c2})}{4C_g} & -\frac{C_{c1}+C_{c2}}{4} & C_q + \frac{C_g}{2} \end{pmatrix}. \quad (3)$$

Inspecting \mathbf{C}_r , one can find that both the matrix elements $[\mathbf{C}_r]_{d,1m}$ and $[\mathbf{C}_r]_{d,2m}$, which describe the coupling between the two qubit modes and the external voltage source, take nonzero values. This means that although in the original circuit, only one of the two qubits is coupled to the voltage source, here, both of the two qubits are coupled to the voltage source simultaneously. As a consequence, after dropping

the free modes, the full circuit shown in Fig. 2(a) can be transformed into an equivalent circuit shown in Fig. 2(b). The most striking result from the equivalence is that due to the presence of the free modes, a spurious microwave crosstalk channel can exist, even if the stray coupling between qubits and drive lines is absent.

To quantify the crosstalk through the spurious channel, we consider the crosstalk strength defined as $M_{ij} \equiv 20 \log_{10}(|\Omega_i/\Omega_j|)$, expressed in units of dB. Here, Ω_j denotes the magnitude of the microwave drive applied to a target qubit (e.g., Q_1), while Ω_i represents the magnitude of the crosstalk felt by the other nearby qubit (e.g., Q_2). For a grounded transmon qubit coupled to an external voltage source V_d via a coupling capacitor C_d , the magnitude of the drive can be approximated by $\Omega = C_d Q_{zpf} V_d / C_q$ with $Q_{zpf} = \sqrt{\hbar/2Z_q}$ the zero-point charge fluctuations and $Z_q = \sqrt{L/C}$ the qubit impedance [30]. L and C correspond to the qubit inductance and capacitance, respectively. For illustration purposes only, we further assume that both qubits have the same qubit inductances and capacitances, thus in the system shown in Fig. 2(a), the strength of the spurious microwave crosstalk from Q_1 to Q_2 can be expressed by

$$M = 20 \log_{10} \left(\left| \frac{[\mathbf{C}_r]_{d,2m}}{[\mathbf{C}_r]_{d,1m}} \right| \right) = 20 \log_{10} (\mathcal{R}), \quad (4)$$

with the ratio \mathcal{R} given by

$$\mathcal{R} = \left| \frac{C_{g4}C_{c1} - C_{g3}C_{c2}}{(C_{g3} + C_{g4})(C_{c2} + C_{g2}) + C_{g2}(C_{c1} + C_{c2})} \right|. \quad (5)$$

As shown in Eq. (5), the spurious crosstalk only depends on the qubit circuit parameters, thus acting as an intrinsic crosstalk channel. Moreover, since in coupled qubit circuits, the coupling capacitors, e.g., C_{c1} and C_{c2} , generally have a rather small capacitance, which is typical of the order of a few fFs or less, the spurious crosstalk can be suppressed through increasing the island capacitance. However, depending on the qubit geometric layout, the island capacitance can take a wide range of values, typically, ranging from a few fFs to 100 fF. Hence, as we will show below, the spurious crosstalk can become non-negligible, thus limiting the performance of qubit addressing.

While here we focus on the direct-coupled qubit system, in Appendices B and C, we also extend the above analysis to the indirect-coupled qubit systems, including floating qubits coupled through a grounded bus or a floating bus. We find that the spurious crosstalk channel disappears for floating qubits coupled via the grounded bus, while it still exists for qubits coupled via the floating bus. This opposite conclusions further demonstrate that the presence of the spurious crosstalk is mediated by the free modes in the qubit circuit. In addition, for floating qubits coupled by the grounded bus, the analysis also shows that the grounded bus can also feel the drive applied to the floating qubit, i.e., a spurious crosstalk channel between the floating qubit and the grounded bus is existent. Thus, we conclude that for the crosstalk from Q_1 to Q_2 in the system shown in Fig. 2(a), this spurious crosstalk is in fact mediated by the free mode supported by the driven qubit Q_1 , and it will still exist even if Q_2 is a grounded one.

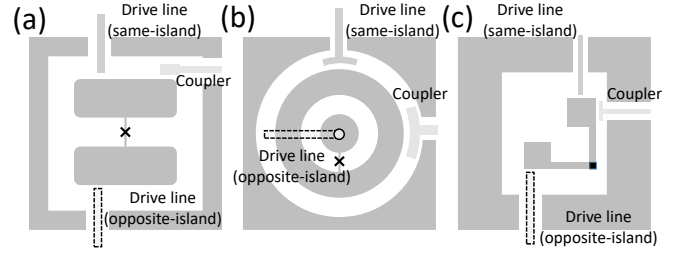


FIG. 3: Different qubit geometric layouts of floating transmon qubits. The drive line (for single-qubit addressing) and coupler (for coupling two qubits) can be coupled capacitively to the same superconducting island or two opposite islands, thus giving rise to two different coupling geometric layouts, i.e., the same-island layout and the opposite-island layout. (a) The typical floating transmon qubit with symmetric islands. (b) The coaxial transmon (coaxmons) with asymmetric islands. (c) The floating merged-element transmon qubit (MET). In (a) and (b), the capacitance between the island and the ground (island capacitance), in general, largely exceeds the coupling capacitor between qubits (coupling capacitance), while in (c) the island capacitance can be comparable with or even be smaller than the coupling capacitance.

TABLE I: Summary of crosstalk (\mathcal{R}) in floating transmon qubits with different qubit geometric layouts. Here $r \equiv C_c/C_g$ denotes the ratio of the coupling capacitance to the island capacitance, and hereafter we refer to it as the capacitance ratio.

| Geometric layout | Asymmetric | Symmetric |
|---|--|---------------------------------|
| | $(\lambda \neq 1)$ | $(\lambda = 1)$ |
| Same-island ($C_{c1} = C_c, C_{c2} = 0$) | $\frac{C_{c1}}{(\lambda + 1)C_g + C_{c1}}$ | $\frac{C_{c1}}{2C_g + C_{c1}}$ |
| | $= \frac{r}{\lambda + 1 + r}$ | $= \frac{r}{2 + r}$ |
| Opposite-island ($C_{c1} = 0, C_{c2} = C_c$) | $\frac{C_{c2}}{(\lambda + 1)\lambda C_g + (2\lambda + 1)C_{c2}}$ | $\frac{C_{c2}}{2C_g + 3C_{c2}}$ |
| | $= \frac{r}{\lambda(\lambda + 1) + (2\lambda + 1)r}$ | $= \frac{r}{2 + 3r}$ |

III. SPURIOUS MICROWAVE CROSSTALK IN TYPICAL FLOATING TRANSMON CIRCUITS

The above discussion indicates that the spurious crosstalk channel is intrinsic, and its strength only depends on the qubit circuit parameters, i.e., the concrete qubit geometric layout. Here, to study this geometric dependence, we consider that for the coupled qubit system shown in Fig. 2(a), $C_{g1} = C_{g3} = C_g$ and $C_{g2} = C_{g4} = \lambda C_g$, thus giving rise to

$$\mathcal{R} = \left| \frac{\lambda C_{c1} - C_{c2}}{(\lambda + 1)(C_{c2} + \lambda C_g) + \lambda(C_{c1} + C_{c2})} \right|. \quad (6)$$

Thus, according to the ratio λ of the two island capacitances (hereafter we refer to it as the island asymmetric ratio), there are two main island geometric layouts for floating transmon qubits, i.e., symmetry layout and asymmetry layout. For ex-

ample, the traditional floating transmon qubits have two same islands [23], as shown in Fig. 3(a), thus acting as a symmetric one, while for the coaxial transmon [24], as shown in Fig. 3(b), its two islands have different geometric designs, thus it belongs to the asymmetric one.

Additionally, note that in principle, the drive line and the coupler (e.g., the capacitors C_{c1} and C_{c2}) could be coupled to one of the two islands or both of the two islands simultaneously, as shown in Fig. 2(a). However, for practically implemented floating qubit circuits, as shown in Fig. 3, generally, the drive line and the coupler are dominantly coupled to one of the two islands. Hence, as shown in Fig. 3, here we consider two coupling geometric layouts, i.e., the drive line could be coupled capacitively to the same island or the opposite island with respect to the coupling island, which is coupled capacitively to the other nearby qubits. For example, in Fig. 2(a), when $C_{c1} \neq 0$ and $C_{c2} = 0$, the coupling geometric layout is a same-island one, while for $C_{c1} = 0$ and $C_{c2} \neq 0$, it is an opposite-island case.

According to the above mentioned island geometric layout (symmetric v.s. asymmetric) and coupling geometric layout (same-island v.s. opposite-island), Table I lists the expressions of the crosstalk strengths for four different qubit geometric layouts. Accordingly, Figure 4 shows the crosstalk strengths as a function of the capacitance ratio r , i.e., the ratio of the coupling capacitance to the island capacitance. As shown in Fig. 4(a), for the traditional floating transmon qubits, where the island capacitance is generally far larger than the coupling capacitance, thus the spurious crosstalk can be entirely suppressed below, e.g., -30 dB, regardless of the coupling geometric layout. However, for the floating merged-element transmon qubit (MET) with a symmetric layout [25], where the island capacitance can be comparable to or even smaller than the coupling capacitance, the spurious channel can become the dominated microwave crosstalk source. In this situation, the magnitude of the spurious crosstalk can even be comparable to that of the target drive. In addition, compared to the case of the same-island layout, qubits with the opposite-island layout, especially for the floating MET qubits, can show a less pronounced spurious crosstalk, typically below -10 dB.

Figure 4(b) shows the spurious crosstalk strength for qubits with the asymmetric island layout. One can find that generally larger island asymmetric ratio λ can mitigate the spurious crosstalk, and can become even more noticeable when taking the opposite-island layout. Thus, for the coaxial transmon shown in Fig. 3(b), when the drive line is coupled to the center island and inter-qubit coupling is realized via the outer island, the spurious crosstalk could be readily suppressed below -50 dB. Moreover, while the spurious channel acts as a significant source of the crosstalk for the MET qubits with the symmetric island layout, by taking the opposite-island layout and increasing the island asymmetric ratio, the spurious crosstalk is promising to be pushed below -25 dB.

Given the state-of-the-art values of the microwave crosstalk in multiqubit quantum processors, typically ranging from -25 dB to -30 dB for neighboring control lines [31, 32], we conclude that: (i) for the traditional floating transmon qubits with symmetric island layout, as shown in Fig. 3(a), the spu-

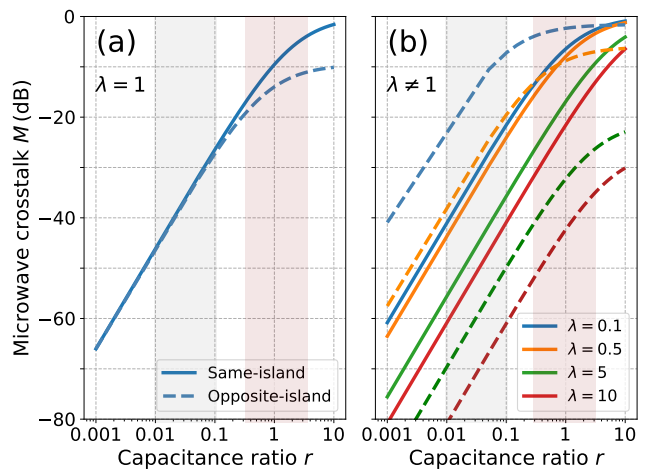


FIG. 4: The spurious crosstalk for coupled floating transmon qubits with different circuit geometric layouts. (a) the spurious crosstalk versus the capacitance ratio r for symmetric qubit geometric layout, i.e., $\lambda = 1$. (b) the spurious crosstalk versus the capacitance ratio r for asymmetric qubit geometric layout, i.e., $\lambda \neq 1$. The solid and dashed lines denote the results for qubit circuits with the two different coupling geometric layouts, i.e., the same-island layout and opposite-island layout, respectively. The gray (light gray) area highlights the ratio band of the typical floating transmon qubits, as shown in Fig. 3(a) and (b), while the pink (gray) area for the floating MET, as shown in Fig. 3(c).

rious crosstalk can be ignored safely if the island capacitance largely exceeds the coupling capacitance. (ii) for the floating transmon qubits with asymmetric island layout, such as the coaxial transmon shown in Fig. 3(b), taking a larger asymmetric ratio could help to suppress the spurious crosstalk. This suppression can become more prominent when employing the opposite-island layout. (iii) for the floating MET qubits with symmetric island layout, as shown in Fig. 3(c), the spurious crosstalk is less readily suppressed. Nevertheless, similar to the coaxial transmon, the combination of the asymmetric island layout and the opposite-island layout will hopefully lead to adequate suppression of the spurious crosstalk.

IV. DISCUSSION

Recently, two independent works show that the free mode can mediate an indirect inter-qubit coupling [26, 27]. In Ref.[26], Sete *et al.* have demonstrated that for qubits coupled via a floating tunable coupler (i.e., an additional frequency-tunable floating transmon qubit), the free mode due to the floating structure of the coupler can induce an indirect inter-qubit coupling, for which its strength only depends on the circuit capacitance, rather than the coupler frequency. Thus, combined with the coupler mediated dispersive coupling, tunable coupling between qubits can be realized by adjusting the coupler frequency [26, 33]. Similarly, in Ref.[27], Yanay *et al.* have shown that in an array of floating transmon qubits,

the free mode can mediate interactions between next-nearest neighbor qubits and even beyond next-nearest neighbors. The strength of the mediated interaction can be engineered via circuit design. Similarly, our results show that the free mode can also mediate cross-driving, enabling the presence of an additional intrinsic crosstalk channel. Hence, our analysis can be viewed as complements to the two earlier works, extending the free-mode mediated interactions from "quantum regime" (for inter-qubit coupling) to "semi-classical regime" (for spurious microwave crosstalk). Moreover, by extending to this semi-classical regime, it is also reasonable to expect that the floating transmon qubit can also relax through the control lines of its coupled neighbors.

V. CONCLUSION

In summary, by performing circuit analysis of two coupled floating transmon qubits, we have demonstrated that the free mode, which is supported by the floating structure of qubits, can induce a spurious microwave crosstalk channel. Depending on the actual qubit geometric layout, the spurious crosstalk can become non-negligible, and can even limit the performance of qubit addressing. Thus, to ensure higher-fidelity qubit addressing, the spurious crosstalk needs to be carefully considered. To address it, we have also shown that for various typical floating transmon circuits, the spurious crosstalk can be largely suppressed through circuit design.

Although our present analysis of the spurious crosstalk focuses on the floating transmon qubits, we expect that the analysis and many of the results may also be applied to other types of superconducting circuits with floating islands, such as flux qubits [34] and fluxonium qubits [35].

Acknowledgments

We acknowledge helpful discussions with Huihai Zhao and Zhenyu Mi. This work was supported by the National Natural Science Foundation of China (Grants No.11890704, No.12104055, No.12004042, No.12104056), the Beijing Natural Science Foundation (Grant No.Z190012), and the Key-Area Research and Development Program of Guang Dong Province (Grant No. 2018B030326001).

Appendix A: Direct Capacitor

Here, we consider two floating qubits coupled via direct capacitors, as shown in Fig. 2(a). The Lagrangian of the circuit can be expressed in terms of the node flux variables Φ_n with $n = \{d, 1, 2, 3, 4\}$, as denoted in Fig. 2(a), and is given as [29]

$$\mathcal{L}' = \frac{1}{2} \dot{\Phi}'^T \mathbf{C}' \dot{\Phi}' + E_{J1} \cos(\phi_1 - \phi_2) + E_{J2} \cos(\phi_3 - \phi_4) \quad (\text{A1})$$

where where E_{J1} and E_{J2} are the Josephson energies, $\phi_n = 2\pi\Phi_n/\Phi_0$ with Φ_0 the magnetic flux quantum, $\Phi' \equiv (\Phi_d \Phi_1 \Phi_2 \Phi_3 \Phi_4)^T$, and \mathbf{C}' the capacitance matrix, given as

$$\mathbf{C}' = \begin{pmatrix} C_d & -C_d & 0 & 0 & 0 \\ -C_d & C_{\Sigma_1} & -C_q & -C_{c1} & 0 \\ 0 & -C_q & C_{\Sigma_2} & 0 & -C_{c2} \\ 0 & -C_{c1} & 0 & C_{\Sigma_3} & -C_q \\ 0 & 0 & -C_{c2} & -C_q & C_{\Sigma_4} \end{pmatrix} \quad (\text{A2})$$

with

$$\begin{aligned} C_{\Sigma_1} &= C_q + C_{g1} + C_{c1} + C_d, \\ C_{\Sigma_2} &= C_q + C_{g2} + C_{c2}, \\ C_{\Sigma_3} &= C_q + C_{g3} + C_{c1}, \\ C_{\Sigma_4} &= C_q + C_{g4} + C_{c2}. \end{aligned} \quad (\text{A3})$$

To identify and remove the free modes in the circuit, we consider the following transformation of the node flux variables with respect to the transformation matrix [28]

$$\mathbf{S} = \begin{pmatrix} 1 & 0 & 0 & 0 & 0 \\ 0 & 1 & 1 & 0 & 0 \\ 0 & 1 & -1 & 0 & 0 \\ 0 & 0 & 0 & 1 & 1 \\ 0 & 0 & 0 & 1 & -1 \end{pmatrix}. \quad (\text{A4})$$

After performing the transformation, the circuit Lagrangian now reads

$$\mathcal{L} = \frac{1}{2} \dot{\Phi}^T \mathbf{C} \dot{\Phi} + E_{J1} \cos(\phi_{1m}) + E_{J2} \cos(\phi_{2m}). \quad (\text{A5})$$

Here, the transformed node flux variables is $\Phi = S\Phi' = (\Phi_d \Phi_{1p} \Phi_{1m} \Phi_{2p} \Phi_{2m})^T$, where $\Phi_{1p(m)} = \Phi_1 \pm \Phi_2$ and $\Phi_{2p(m)} = \Phi_3 \pm \Phi_4$, and the corresponding capacitance matrix is now given as $\mathbf{C} = S^{-1}\mathbf{C}'S^{-1}$. Then, the circuit Hamiltonian can be expressed as [29]

$$H = \sum_j Q_j \dot{\Phi}_j - E_{J1} \cos(\phi_{1m}) - E_{J2} \cos(\phi_{2m}), \quad (\text{A6})$$

where $Q_j = \partial\mathcal{L}/\partial\dot{\Phi}_j$ denotes the charge variable, which is conjugated to the node flux variable Φ_j with $j = \{d, 1p, 1m, 2p, 2m\}$. Here, the modes associated with Q_{1p} and Q_{2p} , and which don't have any potential energies in the circuit Hamiltonian, are the free modes [19–21].

As discussed in previous works, the free modes actually don't participate in the circuit dynamics [19–21]. Hence, one can drop the terms associated with the free modes in the circuit Hamiltonian in Eq. (A6), giving rise to

$$H_r = \frac{1}{2} \mathbf{Q}_r^T \mathbf{C}_r^{-1} \mathbf{Q}_r - E_{J1} \cos(\phi_{1m}) - E_{J2} \cos(\phi_{2m}) \quad (\text{A7})$$

where $\mathbf{Q}_r = (Q_d Q_{1m} Q_{2m})^T$, \mathbf{C}_r denotes the reduced capacitance matrix, which can also be used to describe a system consisting of two direct-coupled grounded transmon qubits, as shown in Fig. 2(b). Here, for illustration purpose and to avoid the extremely cumbersome expression of \mathbf{C}_r , we consider

that all the island capacitor take the same capacitance, i.e., $C_{g1} = C_{g2} = C_{g3} = C_{g4} = C_g$. In this case, the expression of \mathbf{C}_r is given by (since \mathbf{C}_r is a symmetric matrix, hereafter,

$$\mathbf{C}_r = \begin{pmatrix} \tilde{C}_{\Sigma d} & -\frac{C_d C_g (C_{c1} + 2C_g + 3C_{c2})}{K} & -\frac{C_d C_g (C_{c1} - C_{c2})}{K} \\ \blacksquare & \tilde{C}_{\Sigma q1} & -\frac{C_g (C_d + C_g) C_{c2} + C_{c1} (C_g^2 + 4C_{c2} C_g + C_d C_{c2})}{\tilde{C}_{\Sigma q2}} \\ \blacksquare & \blacksquare & \end{pmatrix}, \quad (\text{A8})$$

where

$$K = C_{c1} (C_d + 4C_g) + 4C_g (C_g + C_{c2}) + C_d (2C_g + C_{c2}), \quad (\text{A9})$$

$$\tilde{C}_{\Sigma d} = \frac{4C_d C_g (C_{c1} + C_g + C_{c2})}{K} \quad (\text{A10})$$

$$\begin{aligned} \tilde{C}_{\Sigma q1} = & [C_d (2C_g^2 + (2C_q + 3C_{c2})C_g + C_q C_{c2}) \\ & + C_g (2C_g^2 + (4C_q + 3C_{c2})C_g + 4C_q C_{c2}) \\ & + C_{c1} C_d (C_g + C_q + C_{c2}) \\ & + C_{c1} C_g (3C_g + 4(C_q + C_{c2}))] / K \end{aligned} \quad (\text{A11})$$

$$\begin{aligned} \tilde{C}_{\Sigma q2} = & [C_d (C_g^2 + (2C_q + C_{c2})C_g + C_q C_{c2}) \\ & + C_g (2C_g^2 + (4C_q + 3C_{c2})C_g + 4C_q C_{c2}) \\ & + C_{c1} C_d (C_g + C_q + C_{c2}) \\ & + C_{c1} C_g (3C_g + 4(C_q + C_{c2}))] / K \end{aligned} \quad (\text{A12})$$

When the island capacitance C_g and the shunt capacitance C_q is far larger than the coupling capacitance, i.e., $\{C_g, C_q\} \gg \{C_d, C_{c1}, C_{c2}\}$, the reduced capacitance matrix \mathbf{C}_r can be approximated by

$$\mathbf{C}_r \approx \begin{pmatrix} C_d & -\frac{C_d}{2} & -\frac{C_d(C_{c1} - C_{c2})}{4C_g} \\ -\frac{C_d}{2} & C_q + \frac{C_g}{2} & -\frac{C_{c1} + C_{c2}}{4} \\ -\frac{C_d(C_{c1} - C_{c2})}{4C_g} & -\frac{C_{c1} + C_{c2}}{4} & C_q + \frac{C_g}{2} \end{pmatrix} \quad (\text{A13})$$

Appendix B: Grounded Bus

Here, as shown in Fig. 5(a), we consider that two floating transmon qubits coupled via a grounded bus. Following the same procedure given in Appendix A, the circuit in Fig. 5(a) can be reduced to the circuit in Fig. 5(b), where two grounded transmon qubits are coupled via a grounded bus. After removing free modes, the reduced capacitance matrix of the current circuit is given by (here, the charge variables are $\mathbf{Q}_r = (Q_d Q_{1m} Q_t Q_{2m})^T$, and the corresponding flux variables are $\Phi_r = (\Phi_d \Phi_{1m} \Phi_t \Phi_{2m})^T$ with $\Phi_{1m} = \Phi_1 - \Phi_2$ and $\Phi_{2m} = \Phi_3 - \Phi_4$)

the elements in the lower triangular parts of the capacitance matrix, denoted by \blacksquare , are not given explicitly)

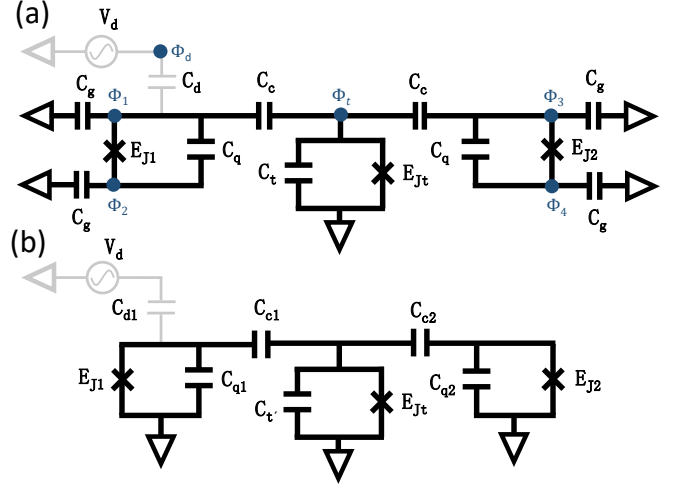


FIG. 5: (a) Schematic circuit diagram for two floating transmon qubits (Q_1 and Q_2) coupled via a grounded bus (Q_B), where a dedicated drive line (left) is coupled capacitively to one of the two qubits, i.e., Q_1 . After removing free modes, the circuit can be transformed into an equivalent circuit shown in (b), where two grounded transmon qubits are coupled via a grounded bus. Note here that unlike the results shown in Fig. 2, the spurious crosstalk between the two qubits disappears, giving rise to $C_{d2} = 0$. This can be explained by the fact that (i) there is no direct coupling between the two qubits; (2) the grounded bus does not support the presence of free mode; Thus, there are no free modes to mediate the spurious crosstalk between the two qubits.

$$\mathbf{C}_r = \begin{pmatrix} \tilde{C}_{\Sigma d} & -\frac{C_d C_g}{C_d + C_c + 2C_g} & -\frac{C_d C_c}{C_d + C_c + 2C_g} & 0 \\ \blacksquare & \tilde{C}_{\Sigma q1} & -\frac{C_c C_g}{C_d + C_c + 2C_g} & 0 \\ \blacksquare & \blacksquare & \tilde{C}_{\Sigma t} & -\frac{C_c C_g}{C_c + 2C_g} \\ \blacksquare & \blacksquare & \blacksquare & \tilde{C}_{\Sigma q2} \end{pmatrix}, \quad (\text{B1})$$

where

$$\begin{aligned}\tilde{C}_{\Sigma d} &= \frac{C_d(C_c + 2C_g)}{C_d + C_c + 2C_g}, \\ \tilde{C}_{\Sigma q1} &= \frac{C_d(C_g + C_q) + C_c(C_g + C_q) + C_g(C_g + 2C_q)}{C_d + C_c + 2C_g}, \\ \tilde{C}_{\Sigma q2} &= \frac{C_c(C_g + C_q) + C_g(C_g + 2C_q)}{C_c + 2C_g},\end{aligned}\quad (\text{B2})$$

and

$$\begin{aligned}\tilde{C}_{\Sigma t} &= \frac{(C_c + 2C_g)(2C_g C_t + C_f(4C_g + C_t))}{(C_c + 2C_g)(C_d + C_c + 2C_g)} \\ &+ \frac{C_d(C_c^2 + (4C_g + C_t)C_c + 2C_g C_t)}{(C_c + 2C_g)(C_d + C_c + 2C_g)}.\end{aligned}\quad (\text{B3})$$

When considering that $\{C_g, C_q, C_t\} \gg \{C_d, C_c\}$, the above matrix can be approximated by

$$\mathbf{C}_r \approx \begin{pmatrix} C_d & -\frac{C_d}{2} & -\frac{C_d C_c}{2C_g} & 0 \\ \blacksquare & C_q + \frac{C_g}{2} & -\frac{C_c}{2} & 0 \\ \blacksquare & \blacksquare & C_t & -\frac{C_c}{2} \\ \blacksquare & \blacksquare & \blacksquare & C_q + \frac{C_g}{2} \end{pmatrix}\quad (\text{B4})$$

As shown in Eq. (B1), for qubits coupled via the grounded bus, the spurious crosstalk disappears, i.e., the matrix element,

which represents the coupling between the drive source V_d and the Q_2 , takes the value of 0, i.e., $[C_r]_{d,2m} = -C_{d2} = 0$. This is to be expected since the grounded bus does not support the presence of free mode, thus there are no free modes to mediate the spurious crosstalk between the two qubits.

In addition, note that the matrix element $[C_r]_{d,t}$ gets a nonzero value, as shown in Eq. (B1). This means that there exists a spurious crosstalk channel between the qubit Q_1 and the grounded bus Q_t (in Fig. 5(b), the corresponding virtual drive line is not presented explicitly). Thus, we can conclude that this spurious crosstalk channel is mediated by the free mode supported by the qubit Q_1 .

Appendix C: Floating Bus

Here, as shown in Fig. 6(a), we consider that two floating transmon qubits coupled via a floating bus [26]. Following the same procedure given in Appendix A, the circuit in Fig. 6(a) can be transformed into an equivalent circuit shown in Fig. 6(b), where two grounded transmon qubits are coupled via a coupler circuit combining a grounded bus and a capacitor [26, 33]. Accordingly, the reduced capacitance matrix of the present circuit is given by (here, the charge variables are $\mathbf{Q}_r = (Q_d Q_{1m} Q_t Q_{2m})^T$, and the corresponding flux variables are $\mathbf{\Phi}_r = (\Phi_d \Phi_{1m} \Phi_t \Phi_{2m})^T$ with $\Phi_{1m} = \Phi_1 - \Phi_2$, $\Phi_t = \Phi_3 - \Phi_4$, and $\Phi_{2m} = \Phi_5 - \Phi_6$)

$$\mathbf{C}_r = \begin{pmatrix} \tilde{C}_{\Sigma d} & -\frac{C_d C_g (2C_b(C_c + 2C_g) + C_c(C_c + 4C_g))}{K} & -\frac{C_c C_d (2C_c C_g + C_b(C_c + 2C_g))}{K} & -\frac{C_c^2 C_d C_g}{K} \\ \blacksquare & \tilde{C}_{\Sigma q1} & -\frac{C_c C_g (2C_c C_g + C_b(C_c + 2C_g))}{K} & -\frac{C_c^2 C_g^2}{K} \\ \blacksquare & \blacksquare & \tilde{C}_{\Sigma t} & \frac{C_c C_g (C_c(C_d + 2C_g) + C_b(C_c + C_d + 2C_g))}{K} \\ \blacksquare & \blacksquare & \blacksquare & \tilde{C}_{\Sigma q2} \end{pmatrix}, \quad (\text{C1})$$

where

$$K = 2C_b(C_c + 2C_g)(C_c + C_d + 2C_g) + C_c(4C_g(C_d + 2C_g) + C_c(C_d + 4C_g)), \quad (\text{C2})$$

$$\tilde{C}_{\Sigma d} = \frac{2C_d(C_c + 2C_g)(2C_c C_g + C_b(C_c + 2C_g))}{K}, \quad (\text{C3})$$

$$\begin{aligned}\tilde{C}_{\Sigma q1} &= [2C_b(C_c + 2C_g)(C_c(C_g + C_q) + C_d(C_g + C_q) \\ &+ C_g(C_g + 2C_q)) + C_c(4C_g(C_d(C_g + C_q) \\ &+ C_g(C_g + 2C_q)) + C_c(C_d(C_g + C_q) \\ &+ C_g(3C_g + 4C_q)))]/K,\end{aligned}\quad (\text{C4})$$

$$\begin{aligned}\tilde{C}_{\Sigma t} &= [(C_c + 2C_g)(C_c + C_d + 2C_g)C_b^2 \\ &+ ((C_d + 4C_g + 2C_t)C_c^2 + 2(4C_g(C_g + C_t) \\ &+ C_d(2C_g + C_t))C_c + 4C_g(C_d + 2C_g)C_t)C_b \\ &+ C_c(4C_g(C_d + 2C_g)C_t + C_c(4C_g(C_g + C_t) \\ &+ C_d(2C_g + C_t)))]/K,\end{aligned}\quad (\text{C5})$$

$$\begin{aligned}\tilde{C}_{\Sigma q2} &= [2C_b(C_c + C_d + 2C_g)(C_c(C_g + C_q) \\ &+ C_g(C_g + 2C_q)) + C_c(2C_g(C_d + 2C_g)(C_g + 2C_q) \\ &+ C_c(C_d(C_g + C_q) + C_g(3C_g + 4C_q)))]/K.\end{aligned}\quad (\text{C6})$$

When considering that $\{C_g, C_q, C_t, C_b\} \gg \{C_d, C_c\}$,

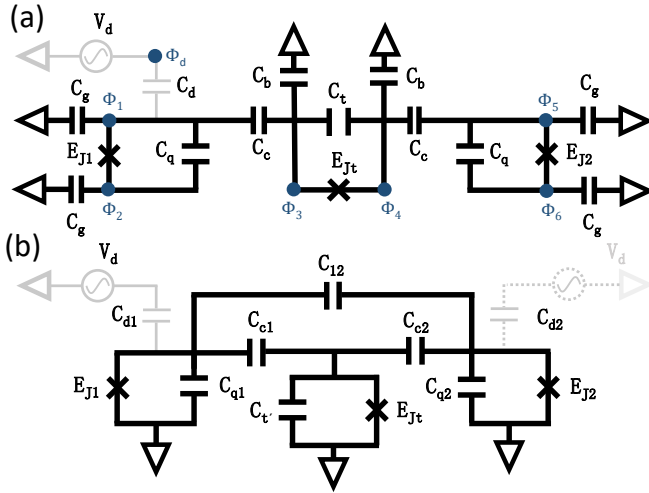


FIG. 6: (a) Schematic circuit diagram for two floating transmon qubits (Q_1 and Q_2) coupled via a floating bus (Q_B), where a dedicated drive line (left) is coupled capacitively to one of the two qubits, i.e., Q_1 . After removing the free modes supported by the floating structure of qubits, the circuit can be transformed into an equivalent circuit shown in (b), where two grounded transmon qubits are coupled via a grounded bus. Here, the spurious crosstalk between the two qubits exists due to the presence of the free mode supported by the floating bus.

the above matrix can be approximated by

$$\mathbf{C}_r \approx \begin{pmatrix} C_d & -\frac{C_d}{2} & -\frac{C_d C_c}{4C_g} & -\frac{C_c^2 C_d}{8C_b C_g} \\ \blacksquare & C_q + \frac{C_g}{2} & -\frac{C_c}{4} & -\frac{C_c^2}{8C_b} \\ \blacksquare & \blacksquare & C_t + \frac{C_b}{2} & -\frac{C_c}{4} \\ \blacksquare & \blacksquare & \blacksquare & C_q + \frac{C_g}{2} \end{pmatrix}. \quad (\text{C7})$$

As shown in Eq. (C1), for qubits coupled via the floating bus, the spurious crosstalk between the two qubits exists due to the presence of the free mode supported by the floating bus. Moreover, as demonstrated in previous works [26, 27], the free mode, which is supported by the floating bus, can also mediate an indirect coupling between the two qubits.

-
- [1] J. M. Martinis, Qubit Metrology for Building a Fault Tolerant Quantum Computer, *npj Quantum Inf.* **1**, 15005 (2015).
- [2] J. Wenner, M. Neeley, R. C. Bialczak, M. Lenander, E. Lucero, A. D. ÓConnell, D. Sank, H. Wang, M. Weides, A. N. Cleland, and J. M. Martinis, Wirebond cross talk and cavity modes in large chip mounts for superconducting qubits, *Supercond. Sci. Technol.* **24**, 065001 (2011).
- [3] J. M. Martinis and A. Megrant, UCSB final report for the CSQ program: Review of decoherence and materials physics for superconducting qubits, [arXiv:1410.5793](https://arxiv.org/abs/1410.5793).
- [4] D. Rosenberg, S. Weber, D. Conway, D. Yost, J. Mallek, G. Calusine, R. Das, D. Kim, M. Schwartz, W. Woods, J. L. Yoder, and W. D. Oliver, 3D integration and packaging for solid-state qubits, [arXiv:1906.11146](https://arxiv.org/abs/1906.11146).
- [5] A.D. Patterson, J. Rahamim, T. Tsunoda, P.A. Spring, S. Jebari, K. Ratter, M. Mergenthaler, G. Tancredi, B. Vlastakis, M. Esposito, and P.J. Leek, Calibration of a Cross-Resonance Two-Qubit Gate Between Directly Coupled Transmons, *Phys. Rev. Appl.* **12**, 064013 (2019).
- [6] S. Huang, B. Lienhard, G. Calusine, A. Vepsäläinen, J. Braumüller, D. K. Kim, A. J. Melville, B. M. Niedzielski, J. L. Yoder, B. Kannan, T. P. Orlando, S. Gustavsson, and W. D. Oliver, Microwave Package Design for Superconducting Quantum Processors, *PRX Quantum* **2**, 020306 (2021).
- [7] D. M. Abrams, N. Didier, S. A. Caldwell, B. R. Johnson, and C. A. Ryan, Methods for Measuring Magnetic Flux Crosstalk between Tunable Transmons, *Phys. Rev. Applied* **12**, 064022 (2019).
- [8] X. Dai, D. M. Tennant, R. Trappen, A. J. Martinez, D. Melanson, M. A. Yurtalan, Y. Tang, S. Novikov, J. A. Grover, S. M. Disseler, J. I. Basham, R. Das, D. K. Kim, A. J. Melville, B. M. Niedzielski, S. J. Weber, J. L. Yoder, D. A. Lidar, and A. Lupascu, Calibration of flux crosstalk in large-scale flux-tunable superconducting quantum circuits, *PRX Quantum* **2**, 040313 (2021).
- [9] J. M. Gambetta, A. D. Córcoles, S. T. Merkel, B. R. Johnson, John A. Smolin, J. M. Chow, C. A. Ryan, C. Rigetti, S. Poletto, T. A. Ohki, M. B. Ketchen, and M. Steffen, Characterization of Addressability by Simultaneous Randomized Benchmarking, *Phys. Rev. Lett.* **109**, 240504 (2012).
- [10] P. S. Mundada, G. Zhang, T. Hazard, and A. A. Houck, Suppression of Qubit Crosstalk in a Tunable Coupling Superconducting Circuit, *Phys. Rev. Applied* **12**, 054023 (2019).
- [11] K. X. Wei, E. Magesan, I. Lauer, S. Srinivasan, D. F. Bogorin, S. Carnevale, G. A. Keefe, Y. Kim, D. Klaus, W. Landers, N. Sundaresan, C. Wang, E. J. Zhang, M. Steffen, O. E. Dial, D. C. McKay, and A. Kandala, Quantum crosstalk cancellation for fast entangling gates and improved multi-qubit performance, [arXiv:2106.00675](https://arxiv.org/abs/2106.00675).
- [12] P. Zhao, K. Linghu, Z. Li, P. Xu, R. Wang, G. Xue, Y. Jin, and H. Yu, Quantum Crosstalk Analysis for Simultaneous Gate Operations on Superconducting Qubits, *PRX Quantum* **3**, 020301 (2022).
- [13] M. Sarovar, T. Proctor, K. Rudinger, K. Young, E. Nielsen, and R. Blume-Kohout, Detecting crosstalk errors in quantum information processors, *Quantum* **4**, 321 (2020).
- [14] Y. Sung, L. Ding, J. Braumüller, A. Vepsäläinen, B. Kannan, M. Kjaergaard, A. Greene, G. O. Samach, C. McNally, D. Kim, A. Melville, B. M. Niedzielski, M. E. Schwartz, J. L. Yoder, T. P. Orlando, S. Gustavsson, and W. D. Oliver, Realization of High-Fidelity CZ and ZZ-Free iSWAP Gates with a Tunable Coupler, *Phys. Rev. X* **11**, 021058 (2021).

- [15] W. Nuerbolati, Z. Han, J. Chu, Y. Zhou, X. Tan, Y. Yu, S. Liu, and F. Yan, Cancelling microwave crosstalk with fixed-frequency qubits, [arXiv:2204.02946](https://arxiv.org/abs/2204.02946).
- [16] F. Solgun, D. DiVincenzo, and J. Gambetta, Simple Impedance Response Formulas for the Dispersive Interaction Rates in the Effective Hamiltonians of Low Anharmonicity Superconducting Qubits, *IEEE Trans. Microw. Theory Tech.* **67**, 928 (2019).
- [17] B. R. Johnson. Controlling Photons in Superconducting Electrical Circuits. PhD thesis, Yale University, May 2011.
- [18] A. Galiutdinov, A. N. Korotkov, and J. M. Martinis, Resonator-zero-qubit architecture for superconducting qubits, *Phys. Rev. A* **85**, 042321 (2012).
- [19] A. J. Kerman, Efficient numerical simulation of complex Josephson quantum circuits, [arXiv:2010.14929](https://arxiv.org/abs/2010.14929).
- [20] D. Ding, H.-S. Ku, Y. Shi, and H.-H. Zhao, Free-mode removal and mode decoupling for simulating general superconducting quantum circuits, *Phys. Rev. B* **103**, 174501 (2021).
- [21] J. Long, Superconducting Quantum Circuits for Quantum Information Processing. PhD thesis. University of Colorado, Boulder, 2020.
- [22] J. Koch, T. M. Yu, J. Gambetta, A. A. Houck, D. I. Schuster, J. Majer, A. Blais, M. H. Devoret, S. M. Girvin, and R. J. Schoelkopf, Charge-insensitive qubit design derived from the cooper pair box, *Phys. Rev. A* **76**, 042319 (2007).
- [23] H. Paik, S. Srinivasan, S. Rosenblatt, J. Chavez-Garcia, D. Bogorin, O. Jinka, G. Keefe, D. Shao, J.-B. Yau, M. Brink, and J. M. Chow, Coupler characterization of superconducting transmons qubits for cross-resonance gate, *2020 IEEE International Electron Devices Meeting (IEDM), 2020*, pp. 38.2.1-38.2.4.
- [24] J. Rahamim, T. Behrle, M. J. Peterer, A. Patterson, P. A. Spring, T. Tsunoda, R. Manenti, G. Tancredi, and P. J. Leek, Double-sided coaxial circuit QED with out-of-plane wiring, *Appl. Phys. Lett.* **110**, 222602 (2017).
- [25] H. J. Mamin, E. Huang, S. Carnevale, C. T. Rettner, N. Arellano, M. H. Sherwood, C. Kurter, B. Trimm, M. Sandberg, R. M. Shelby, M. A. Mueed, B. A. Madon, A. Pushp, M. Steffen, and D. Rugar, Merged-Element Transmons: Design and Qubit Performance, *Phys. Rev. Appl.* **16**, 024023 (2021).
- [26] E. A. Sete, A. Q. Chen, R. Manenti, S. Kulshreshtha, and S. Poletto, Floating Tunable Coupler for Scalable Quantum Computing Architectures, *Phys. Rev. Appl.* **15**, 064063 (2021).
- [27] Y. Yanay, J. Braumüller, T. P. Orlando, S. Gustavsson, C. Tahan, and W. D. Oliver, Mediated Interactions beyond the Nearest Neighbor in an Array of Superconducting Qubits, *Phys. Rev. Appl.* **17**, 034060 (2022).
- [28] Y. Yanay, J. Braumüller, S. Gustavsson, W. D. Oliver, and C. Tahan, Two-dimensional hard-core Bose-Hubbard model with superconducting qubits, *npj Quantum Inf.* **6**, 58 (2020).
- [29] U. Vool and M. Devoret, Introduction to quantum electromagnetic circuits, *Int. J. Circuit Theory Appl.* **45**, 897 (2017).
- [30] D. T. Sank, Fast, accurate state measurement in superconducting qubits, Ph.D. thesis. University of California, Santa Barbara, 2014.
- [31] M. Gong, S. Wang, C. Zha, M.-C. Chen, H.-L. Huang, Y. Wu, Q. Zhu, Y. Zhao, S. Li, S. Guo *et al.*, Quantum walks on a programmable two-dimensional 62-qubit superconducting processor, *Science* **372**, 948 (2021).
- [32] W. Ren, W. Li, S. Xu, K. Wang, W. Jiang, F. Jin, X. Zhu, J. Chen, Z. Song, P. Zhang *et al.*, Experimental quantum adversarial learning with programmable superconducting qubits, [arXiv:2204.01738](https://arxiv.org/abs/2204.01738).
- [33] F. Yan, P. Krantz, Y. Sung, M. Kjaergaard, D. L. Campbell, T. P. Orlando, S. Gustavsson, and W. D. Oliver, Tunable Coupling Scheme for Implementing High-Fidelity Two-Qubit Gates, *Phys. Rev. Appl.* **10**, 054062 (2018).
- [34] T. P. Orlando, J. E. Mooij, L. Tian, Caspar H. van der Wal, L. S. Levitov, S. Lloyd, and J. J. Mazo, Superconducting persistent-current qubit, *Phys. Rev. B* **60**, 15398 (1999).
- [35] V. E. Manucharyan, J. Koch, L. I. Glazman, and M. H. Devoret, Fluxonium: Single Cooper-pair circuit free of charge offsets, *Science* **326**, 113 (2009).